Nano Energy 90 (2021) 106566

Contents lists available at ScienceDirect

Nano Energy

journal homepage: www.elsevier.com/locate/nanoen

Full paper

A liquid-free poly(butylene oxide) electrolyte for near-room-temperature and 4-V class all-solid-state lithium batteries

Jing Luo [a], Qian Sun [a], Jianneng Liang [a], Xiaofei Yang [a], Jianwen Liang [a], Xiaoting Lin [a], Feipeng Zhao [a], Yulong Liu [a], Huan Huang [b], Li Zhang [c], Shangqian Zhao [c], Shigang Lu [c], Ruying Li [a], Xueling Sun [a,*]

[a] Department of Mechanical and Materials Engineering, University of Western Ontario, 1151 Richmond St, London, Ontario, Canada N6A 3K7
[b] Glabat Solid-State Battery Inc., 700 Collip Circle, London, ON, Canada N6G 4X8
[c] China Automotive Battery Research Institute Co. Ltd, 5th Floor, No. 43, Mining Building, North Sanhuan Middle Road, Beijing 100088, China

ARTICLE INFO

Keywords:
Solid polymer electrolyte
Solid-state batteries
4-V class cathodes
Poly(butylene oxide)
Poly(tetrahydrofuran)

ABSTRACT

Solid polymer electrolyte (SPE) is a promising class of solid electrolytes for building All-solid-state lithium batteries (ASSLBs) due to their flexibility and compatibility with electrodes. However, the requirement of an elevated operating temperature (> 60 °C) and the high-voltage instability remain major drawbacks for the most commonly used poly(ethylene oxide) (PEO) SPEs. Alternatively, poly(butylene oxide) (PBO) is another member of the polyether family that shows significantly enhanced ionic conductivity at room temperature, but its application in ASSLBs is rarely investigated, probably due to challenges of engineering methodology and interfacial stability. Herein, we develop a solvent-free fabrication route for building PBO SPE membrane for application in ASSLBs with feasible performance near room temperature. We demonstrate a facile activation methodology to stabilize the electrode/electrolyte interface for the PBO based ASSLBs. As a result, the ASSLB with a $LiFePO_4$ cathode delivers a stable specific capacity of ~ 140 mA h g^{-1} at 0.1 C with almost 100% retention after 100 cycles near room temperature. Moreover, despite the poor high-voltage stability of PEO, we found that the PBO SPE presents good compatibility with 4-V class cathodes without any additional coating, achieving a capacity retention of 94.6% over 100 cycles with a conventional $LiCoO_2$ cathode at 60 °C. This work shall inspire new possibilities of dry SPEs development for ASSLBs.

1. Introduction

All-solid-state lithium batteries (ASSLBs) are attracting increasing research interests due to their unique advantages in safety and energy density over conventional Li-ion batteries (LIBs) [1]. Considering from a comprehensive perspective including compatibility with electrodes, durability, ionic conductivity, and processability, the mechanically flexible solid polymer electrolytes (SPEs) with an adequate ionic conductivity are closest to commercialization [2–6]. Particularly, a solid-state battery based poly(ethylene oxide) (PEO) SPE has been commercialized to power the Bluecar electric vehicles by Bolloré, which demonstrates a successful model using a $LiFePO_4$/SPE/Li-metal battery. However, the PEO based SPEs must operate at an elevated temperature within 60–80 °C, which requires external heating equipment and extra energy and thus remains a major constrain [4,7].

Functionality at ambient temperature becomes an important topic for building next-generation ASSLBs. Extensive research efforts are dedicated to improving the ionic conductivity of SPEs, ideally above 10^{-4} S cm^{-1} at room temperature, for practical applications [1]. To overcome the intrinsically low room-temperature ionic conductivity (~ 10^{-8} S cm^{-1}) of PEO-based SPEs, some common approaches are proposed, such as (1) introduction of small molecular plasticizers, ceramic fillers, and/or block-copolymers to enhance the amorphous phase for ion hopping conduction [4,8], (2) development of single-ion conductors [9,10], (3) incorporation of novel lithium salts [11], and (4) synthesis of novel polymers such as polymeric ionic liquid [12]. Nevertheless, most batteries based on the reported SPEs in previous works have yet demonstrated practical performance near room temperature, especially for the liquid/solvent-free SPEs. To another extent, gel polymer electrolytes which intentionally incorporate liquid

* Corresponding author.
E-mail address: xsun9@uwo.ca (X. Sun).

https://doi.org/10.1016/j.nanoen.2021.106566
Received 4 August 2021; Received in revised form 12 September 2021; Accepted 22 September 2021
Available online 1 October 2021

electrolytes or organic solvents into the SPE matrixes could deliver excellent room-temperature performance [13,14], but the introduction of liquid phase(s) may lead to similar safety concerns as those of liquid electrolyte based LIBs. In fact, even minor addition of organic plasticizers or incomplete drying of the casting solvents could lead to a speciously high room-temperature ionic conductivity due to the gel polymer electrolyte characteristics [15,16]. However, it is difficult to achieve a high room-temperature ionic conductivity when the SPE is completely dried.

Due to the structural similarity between poly(butylene oxide) (PBO, $[–CH_2CH_2CH_2CH_2O–]_n$ [17,18], also known as poly(tetrahydrofuran), PTHF [19–21]) and PEO ($([–CH_2CH_2O–]_n$), some previous studies had attempted to explore PBO as a potential SPE candidate to replace PEO. The linear PBO polymer intrinsically possesses a lower melting point than that of PEO. The longer alkane moiety between the functional oxygens can lead to loose Li^+ coordination and facilitate Li^+ conduction [19]. Actually, PBO based SPEs have demonstrated an attractive ionic conductivity in the order of 10^{-4} S cm^{-1} at ~ 25 °C in the early references about two decades ago. However, their application and/or electrochemical performance in a ASSLB system has not been reported until recently [22–25]. Cui et al. firstly demonstrated a PTHF/UV-curable polymer blend SPE with advantages of a loosely coordinating SPE, meanwhile addressing the poor mechanical properties and thermal instability concern by UV assisted crosslinking. However, the crosslinked PTHF SPE ionic conductivity near room-temperature was low (1.5×10^{-6} S cm^{-1} at 30 °C), and this SPE system still required an addition of 18 wt% liquid plasticizers (e.g. *N,N*-dimethylformamide or propylene carbonate) to enable tentative room-temperature operation [19]. More recently, G. Cui et al. reported in-situ polymerization of tetrahydrofuran in a cellulose support to synthesize a PTHF-based SPE that showed adequate compatibility with lithium metal at 60 °C in the presence of the BF_3 initiator. However, they found that the resulted SPE still contained 33.3 wt% of small molecular weight component as plasticizer by nuclear magnetic resonance (NMR) [21]. While their NMR analysis showed no small molecular weight component in the commercial PBO (i.e. PTHF) sample, the ASSLB using a SPE based on the commercial PBO polymer failed to achieve good electrochemical performance even at 60 °C, neither room-temperature performance was reported in this work. Therefore, there are severe challenges yet to be solved for realizing a successful PBO based SPE for feasible ASSLB performance at near room temperatures. Moreover, an effective strategy to achieve a favorable dry SPE without plasticizers also remains to be explored.

In this work, we develop a solvent-free fabrication route for building a PBO SPE membrane for application in ASSLB with feasible performance at near room temperature without adding any solvents or plasticizers. Specifically, omitting the use of a casting solvent, the PBO SPE herein is prepared by directly dissolving a lithium salt into the molten PBO polymer at an elevated temperature and subsequently solidifying in a glass fiber support during cooling. While the PBO SPE exhibits comparable performance to the state-of-the-art PEO SPE at 60 °C, the room-temperature performance surpass PEO. The $LiFePO_4$ battery using the PBO SPE delivers a stable specific capacity of ~ 140 mA h g^{-1} at 0.1 C for 100 cycles with almost 100% retention at room temperature (~ 28 °C). Meanwhile, we demonstrate a facile activation methodology to stabilize the interface between electrode and electrolyte in the PBO based ASSLBs. We found that an electrochemical activation at an elevated temperature can facilitate in-situ formation of a favorable cathode electrolyte interphase (CEI) with rich LiF and Li_2O on the cathode surface that is crucial for room-temperature cycling stability. In addition, unlike the poor high-voltage stability of PEO, the PBO SPE possesses good intrinsic stability towards 4-V class cathodes, achieving a capacity retention of 94.6% with a conventional $LiCoO_2$ cathode over 100 cycles at 60 °C. The near-room-temperature performance and electrochemical stability demonstrated by the PBO based SPE shall inspire rethinks of the possibilities of dry SPEs excluding plasticizer additives.

2. Results and discussion

Owing to the low melting point and low viscosity of PBO, the PBO based SPE can be prepared using a solvent-free method by directly dissolving the bis(trifluoromethanesulfonyl)imide lithium salt (LiTFSI) into molten PBO at 75 °C. The stoichiometric [BO]:Li^+ ratios are chosen as 4, 6, 8, 12, and 16:1, respectively. Waxy-white PBO SPE membranes were readily obtained after impregnating the molten electrolyte into a glass fiber support and cooling to room temperature (inset in Fig. 1a). Notably, the PBO SPE was non-volatile and not flowable at room temperature (Fig. S1), but the wax-like property required mechanical strengthening to ensure the form during coin cell assembly.

The dissociation of lithium salt and transformation of PBO from highly crystalline to mainly amorphous can be revealed by X-ray diffraction (XRD) and Raman characterizations. As shown in Fig. 1a, pure PBO polymer was highly crystalline at room temperature, showing strong characteristic XRD peaks at $2\theta = 19.6°$ and 24.1°; the lower-angle peak convoluted two close peaks at $2\theta = 19.4°$ and 19.7° (ICSD no. 00-062-1708). The minor XRD peaks at higher angles were also exactly indexed to the crystalline PBO. In contrast, the crystallinity of PBO sharply decreased in the SPE, appearing mainly amorphous with a trace amount of crystalline domains. Meanwhile, while the LiTFSI salt was also highly crystalline in its pure form, the characteristic XRD peaks were essentially absent after dissolving the salt into the PBO polymer matrix to form SPE, indicating the dissociation of LiTFSI. Moreover, the solvation of LiTFSI and complex with PBO can be further verified by Raman analysis. As shown in Fig. 1b, the strong band near 746 cm^{-1} was due to Raman mode of $TFSI^-$ anions in the PBO SPE. Deconvolution of this peak identified the signals from ion pairs at 746.1 cm^{-1} and free ions at 741.2 cm^{-1} [26–28]. Presumably, the ion pairs were weakly associated locally rather than precipitation of salt aggregates which should have a strong Raman signal at 749 cm^{-1} [24,27].

Fig. 1c shows the temperature-dependent ionic conductivity of PBO SPEs at different salt concentrations ranging from [BO]:Li^+ ratios of 4:1–16:1. Generally, these SPEs appeared to have a threshold temperature, above which their ionic conductivities displayed a typical Arrhenius behavior [4,29]. Interestingly, the PBO SPEs with a higher salt concentration demonstrated a lower temperature threshold but a higher activation energy for ion motion (Fig. S2). By differential thermal analysis, the heat flow curves indicated a slightly higher melting point (T_m) than the threshold temperature (Fig. S3). For example, at a [BO]:Li^+ ratio of 8:1, the T_m of 39 °C is above the threshold temperature of 23 °C. And the glass transition temperature of PBO polymer is below − 80 °C which is well beyond the temperature range of battery operation [30–32]. To better understand the ion association effects on the threshold temperature, Raman spectra of the PBO SPEs of different salt concentrations were compared at 25 °C and at a molten state at 70 °C. Overall, as consistent with the salt concentrations, the Raman spectra for the PBO SPEs with an increasing [BO]:Li^+ ratio showed a decrease in the intensity of the $TFSI^-$ characteristic Raman bands relative to those related to the PBO polymer chains (Fig. S4). However, the fraction of free $TFSI^-$ ions was more dependent on the temperature rather than the salt concentration (Fig. S5). Therefore, the threshold temperature should be related to the effective number of Li^+ ions coordinated per [BO] unit (Fig. S6) together with the enhanced PBO segmental motion upon increasing temperature [1,4].

Among all PBO SPEs, the [BO]:Li^+ ratio of 8:1 exhibited an optimal ionic conductivity of 1.4×10^{-5} S cm^{-1} at 25 °C and an acceptable threshold temperature of 23 °C for near-room-temperature operations. Therefore, this salt concentration was used for the rest of the study. Fig. 1d schematically depicts the dissociation of lithium salt and reorganization of the crystalline polymer to form highly amorphous ion-polymer complexes for good Li^+ conduction near room temperature. As additional advantages, such a solvent-free process not only avoids the

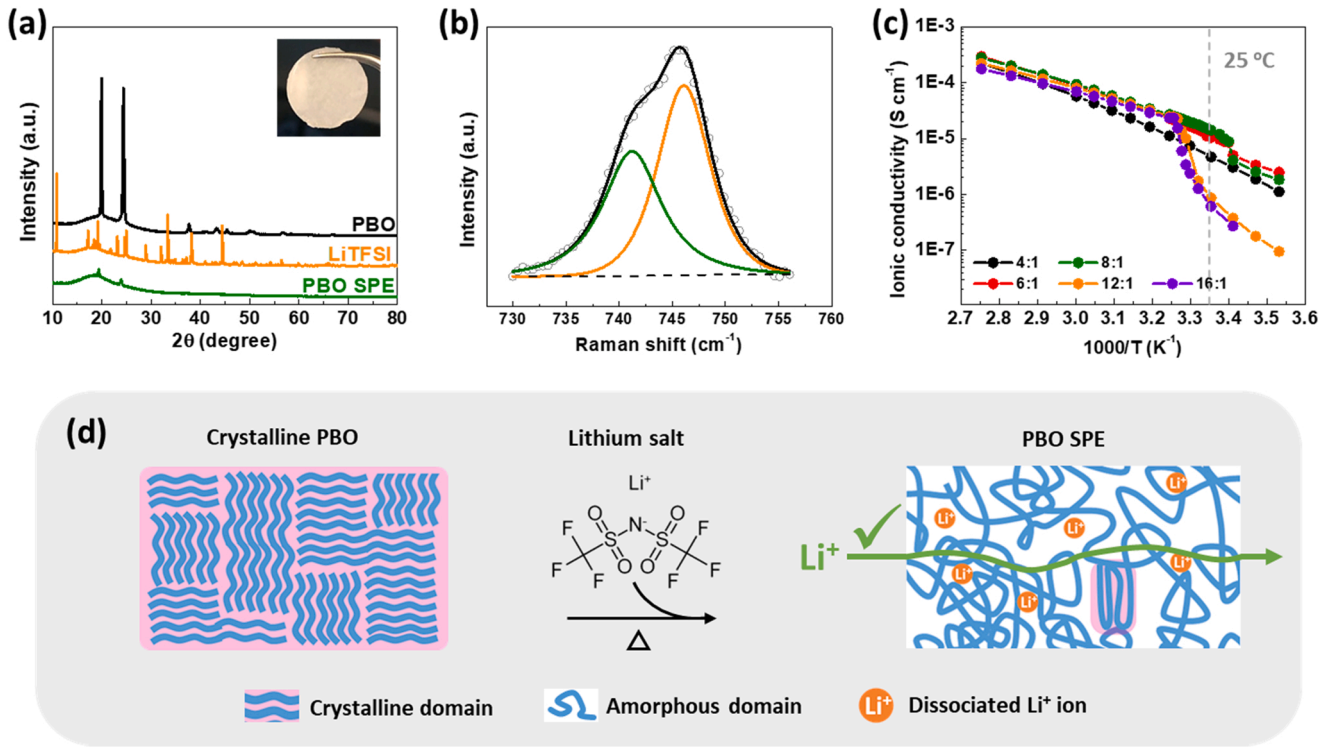

Fig. 1. Characterization of the PBO electrolyte. (a) XRD patterns of pure PBO, pure LiTFSI salt, and the PBO SPE containing dissolved LiTFSI in PBO ([BO]:Li^+ = 8:1); inset is an optical image of the PBO SPE membrane at room temperature. (b) Raman spectrum (symbols) of the PBO SPE ([BO]:Li^+ = 8:1); solid lines show the fitted functions for free ions (green), ion pairs (orange), and their sum (black). (c) Temperature dependent ionic conductivities at various [BO]:Li^+ ratios. (d) Schematic illustration of crystalline PBO in pure form and amplified amorphous regime after dissolving lithium salt and self-reorganization; the enhanced amorphous phase promotes high ambient ionic conductivity of PBO electrolyte.

usage of toxic organic solvents but also eliminates possible influences of residual solvent during electrochemical characterizations. Moreover, the as-prepared PBO SPE possessed good thermal stability up to 248 °C (Fig. S7), which fulfills the requirement for safe LIB operation [19]. The PBO SPE also exhibited a high transference number of 0.62 ± 0.04 (Fig. S8), while common PEO based SPEs usually has a low transference number around 0.2 [1,19]. The higher transference can be attributed to the looser O–Li^+ interaction in the PBO system, whereas the stronger O–Li^+ coordination in the PEO system can trap Li^+ in a bound state that hinders fractional mobility of Li^+ cations [19,33].

Using $LiFePO_4$ (LFP) as the cathode and lithium metal as the counter electrode, the PBO SPE was sandwiched in between to test battery performance in an ASSLB configuration. At an elevated temperature of 60 °C, the PBO electrolyte demonstrated comparable performance to the state-of-the-art PEO based SPE (Figs. 2a and S9) [4,34]. The PEO based SPE also had an O:Li^+ ratio of 8:1 and an additional 12 wt% of LLZTO particles for enhancement in ionic conductivity and mechanical properties. The rapid capacity fading of the PEO cell at 2 C was due to the large voltage polarization of PEO and cutoff of discharging voltage plateau near the operating voltage window (Fig. S10). Nevertheless, the performance of the PEO based SPEs are still limited at lower temperatures, not to mention room temperature. In contrast, the cell using PBO SPE demonstrated remarkable cycling performance at room temperature (Fig. 2b). The PBO cell delivered stable capacities of ~ 140 mA h g^{-1} for 100 cycles with almost 100% capacity retention at 0.1 C. The average Coulombic efficiency was as high as 99.8%. As shown in Fig. 2c, the highly overlapped charge-discharge profiles during cycling test indicated an excellent internal stability of the cell. Neither obvious capacity fading, nor voltage polarization was observed. In addition, the discharging rate capability is shown in Fig. 2d. A reasonable discharge capacity above 90 mA h g^{-1} was obtained at a discharging rate of 0.5 C. These results readily surpass the performance delivered by the UV crosslinked electrolyte using a similar base polymer with plasticizers [19].

Interestingly, we found that an effective activation process had played an important role in the good performance near room temperature demonstrated above. Those ASSLBs were subject to 4 pre-cycles at 0.1 C at 60 °C before cycling at room temperature. Fig. 3a compares the cycling performance of cells with or without pre-cycling activation. Unlike the stable performance demonstrated by the pre-cycled cell, no matter directly cycling at room temperature or resting the cell at 60 °C for 16 h before cycling delivered similarly poor performance with rapid capacity fading. This highlights that the activation process underwent an electrochemical route rather than a chemical or physical route. Otherwise, resting at the molten state of PBO electrolyte at 60 °C should had facilitated wetting and impregnation of the SPE into the cathode for improved performance. Some subtle differences should had occurred during the initial cycling at 60 °C versus room temperature.

Fig. 3b and c compare the electrochemical impedance spectra (EIS) of the LFP/PBO SPE/Li cells during the initial charge at 30 °C versus 60 °C. As labeled on the voltage profiles, the EIS were collected after a total charging time of 1, 3, 5, and 7 h at a current density of 0.1 C. Upon initial charging at 30 °C (Fig. 3b), the high-frequency impedance remained unchanged, indicating that the PBO SPE was stable in bulk; however, the significantly increasing electrode impedance at low frequencies suggested a possible continuous augmentation in the cathode interfacial resistance. Presumably, an undesired CEI was formed with insulating products. In great contrast, the EIS during the initial charging at 60 °C were readily stable without obvious changes for the SPE bulk or the electrodes. Hence, either the system was highly stable in its native form, or a favorable CEI was preferentially formed at an elevated temperature.

In order to understand the different CEI chemistries, LFP cathodes were collected from the cells after direct cycling at room temperature

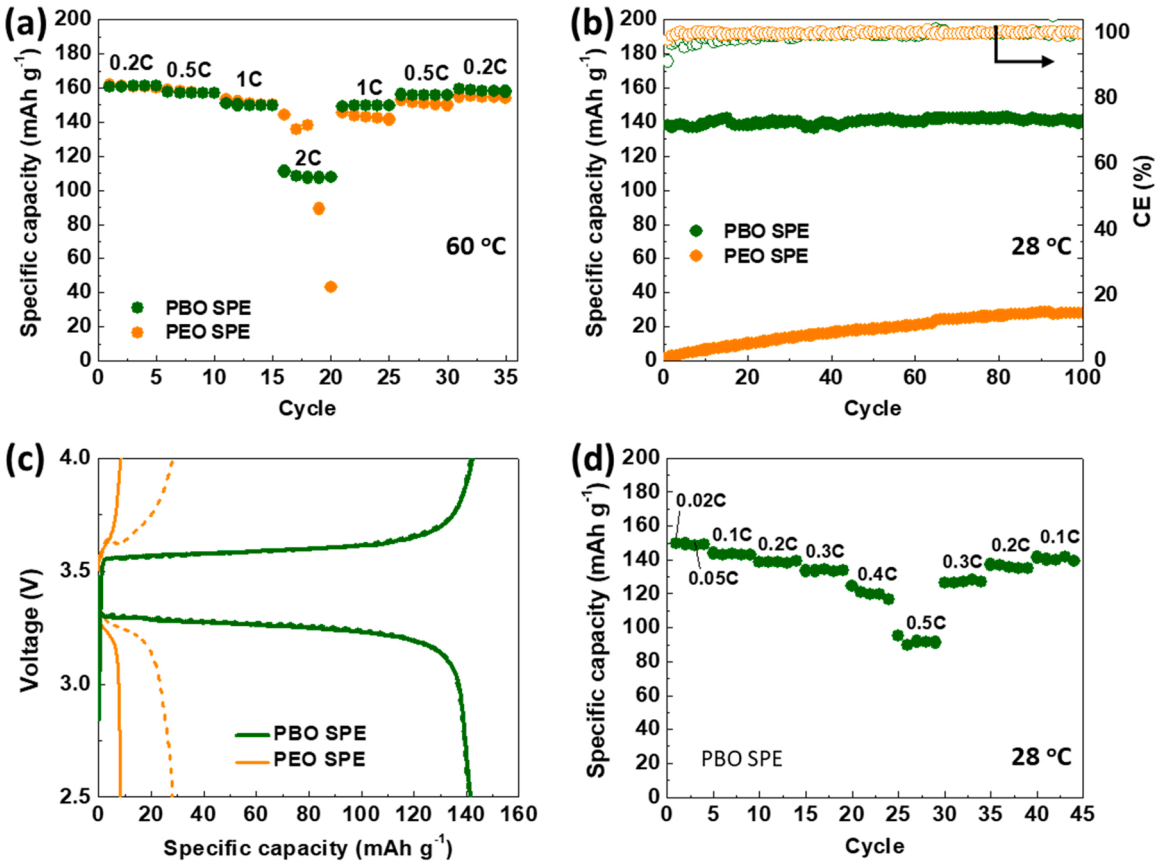

Fig. 2. Electrochemical performance. (a) Comparable rate performance of the LFP/PBO SPE/Li and the LFP/PEO SPE/Li cells at 60 °C; note, the PBO electrolyte was molten at 60 °C. (b) Cycling performance of the LFP/PBO SPE/Li and the LFP/PEO SPE/Li cells at a current density of 0.1 C at near room temperature (~ 28 °C); (c) corresponding charge-discharge profiles at the 15th (solid) and the 100th (dashed) cycles. (d) Discharging rate performance of the LFP/PBO SPE/Li cell at room temperature; for rates above 0.1 C, the cell was always charged at 0.1 C to fully assess the discharging capability.

(LFP-RT) or 60 °C (LFP-60) for X-ray photoelectron spectroscopy (XPS) analyses (Fig. 3d). XPS results for the as-prepared PBO SPE were also measured for reference. For all three samples, the peaks positioned at 55.5 eV in the Li1s spectra, 688.3 eV in the F1s spectra, and 168.4 eV ($S2p_{3/2}$) in the S2p spectra were attributed to the complexed LiTFSI salt in the SPE [35,36]; the peak at 532.2 eV in the O1s spectra was due to the functional oxygen on the PBO backbone. Additional features on the spectra for the LFP cathodes should give hints for the CEI chemistries. For both LFP-RT and LFP-60, the extra peak at 684.5 eV in the F1s spectra along with the contribution at 54.9 eV in the Li1s spectra indicated the formation of LiF, presumably due to partial decomposition of the LiTFSI salt. Signs of Li_2SO_3 around 166.7 eV ($S2p_{3/2}$) in the S2p spectra also provided evidence for the salt decomposition [35,36]. Notably, in addition to the higher relative content of LiF on the LFP-60 than the LFP-RT, another distinct feature for the LFP-60 was observed in the O1s spectrum, where a shoulder at 531.3 eV indicated the presence of Li_2O [37]. It is possible that, at an elevated temperature, the LiTFSI salt preferentially decomposed to form a favorable CEI with rich LiF and Li_2O which stabilized the interface for subsequent cycles (Scheme 1) [38]. Meanwhile, the terminal hydroxyl group of the PBO polymer could have been oxidized into –COOH (Li) with the formation of Li_2O so that PBO polymers with the more stable $–OCH_3$ terminal groups would further improve the high-voltage stability for future PBO-based SPEs [39].

In addition to the feasible battery performance near room temperature, the high-voltage stability of the SPE determines its capability of integrating high-voltage cathodes for high energy density. According to the anodic linear sweep voltammogram (LSV) using a stainless-steel electrode (Fig. S11), the PBO SPE exhibited electrochemical stability up to 5.2 V versus Li/Li^+, significantly higher than typical PEO based SPEs and most reported 'dry' SPEs. However, the massive decomposition of SPEs has been reported to start at a much lower voltage in the presence of high-surface-area conductive materials (3.8 versus 4.5 V for a typical PEO based SPE) [40]. Therefore, the electrochemical stability of our PBO SPE was also evaluated in an actual battery configuration by incrementally increasing the upper voltage limit of the LFP/PBO SPE/Li cell at 60 °C. As shown in Fig. 4a and b, the cell was highly stable up to 4.35 V, above which the flattening of voltage profile was a sign of side reactions. If further pushing the upper voltage limit to 4.5 V, the cell could barely finish charging (Fig. S12), probably due to continuous SPE decomposition. This electrochemical stability response was similar to the result of the anodic LSV using a high-surface-area carbon electrode [41] for a tolerance up to ~ 4.3 V versus Li/Li^+ (Fig. S13). Nevertheless, the PBO SPE already demonstrated a superior high-voltage stability compared to a typical PEO SPE. Under the same testing conditions with a LFP cathode upon incremental upper voltage limits, the cell using PEO based SPE was susceptible to capacity fading and polarizations upon upper voltage limits beyond 4.1 V (Fig. 4d).

To further confirm the electrochemical stability of the PBO SPE within the determined voltage range, long-term cycling performance was evaluated. Fig. 4c shows the cycling performance of the LFP/PBO SPE/Li cell in a voltage window of 2.5–4.3 V operating with a slow-charge/fast-discharge (0.2 C/0.5 C) protocol at 60 °C. A high specific capacity of 150.1 mA h g^{-1} was maintained with a high capacity retention above 90% after 200 cycles. At the same time, stable cycling performance was also demonstrated with a high-voltage $LiCoO_2$ (LCO) cathode in the voltage range of 2.8–4.2 V at 60 °C, achieving a specific capacity of 120.5 mA h g^{-1} and a retention of 95% after 100 cycles at

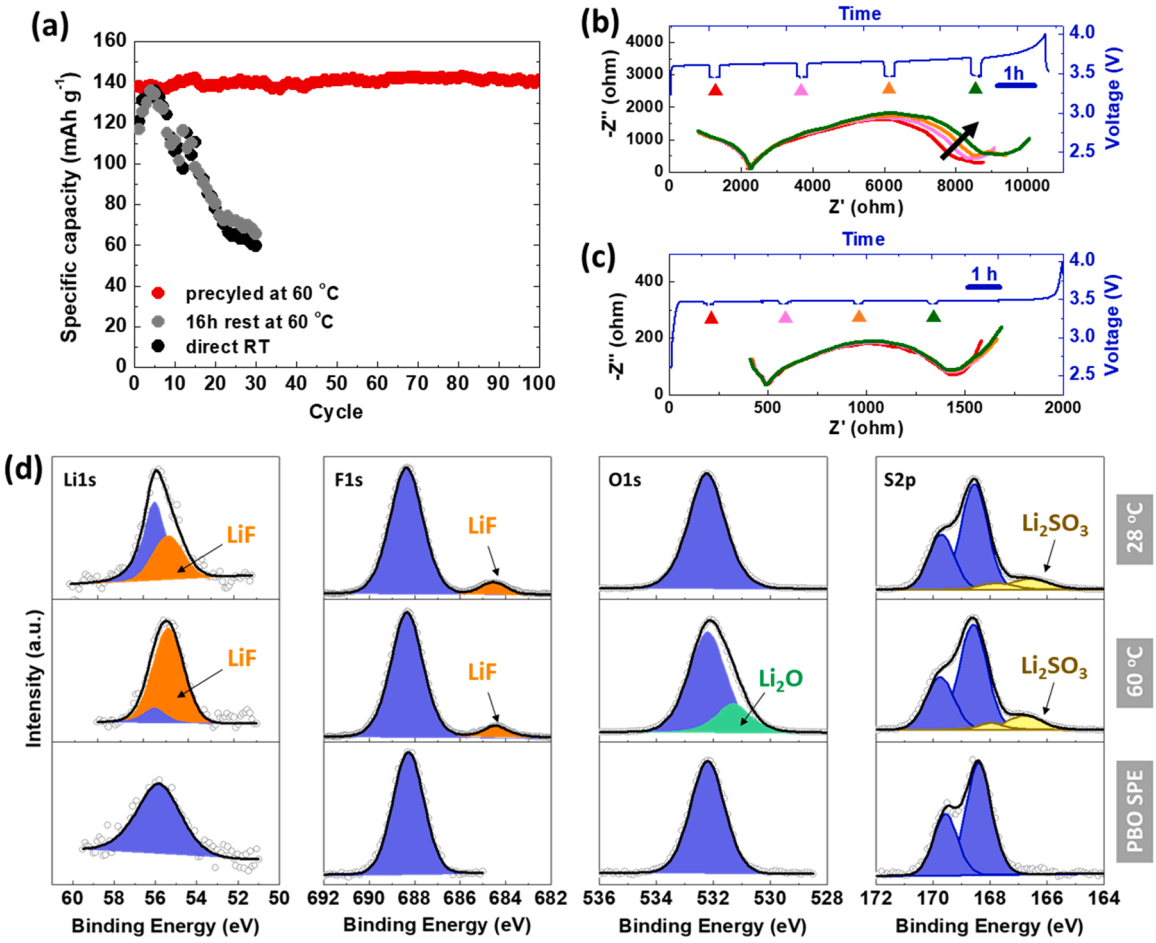

Fig. 3. Effects of pre-cycling activation. (a) Comparison on cycling performance of LFP/PBO SPE/Li cells at 0.1 C and room temperature (~ 28 °C) with or without electrochemical activation at 60 °C. EIS measurements of LFP/PBO SPE/Li cells during the first charge at 0.1 C at (b) 30 °C and (c) 60 °C; the measuring states of charge are labeled on the voltage profiles. (d) XPS spectra showing the elemental fittings from the LFP cathode surface after 10 direct cycles at room temperature (top row) or 4 cycles at 60 °C (middle row); corresponding elemental spectra of the as-prepared PBO SPE (bottom row) are provided for comparison.

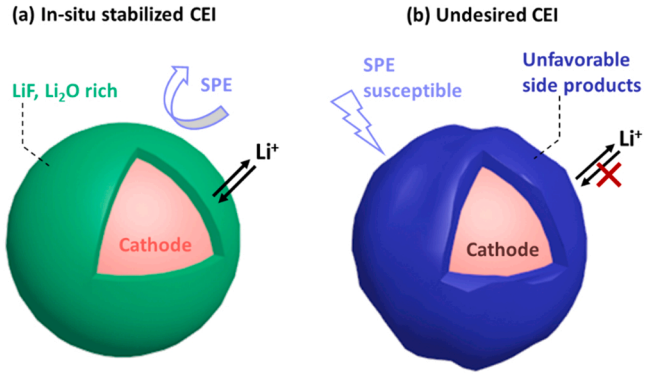

Scheme 1. Schematic illustrations showing (a) a favorable in-situ formed CEI and (b) continuous decomposition of SPE on the unfavorable cathode surface.

0.2 C (Fig. 4e). As shown in Fig. S14a, no obvious polarization was observed in the discharge voltage profiles of the LCO cell, indicating a highly stable internal cell resistance. Moreover, the PBO SPE can also be directly integrated with the attractive $LiNi_{0.8}Mn_{0.1}Co_{0.1}O_2$ (NMC811) cathode and stable up to 4.3 V without any additional surface coating, delivering good cycling performance at 28 °C (Fig. 4e). Presumably, a similar favorable CEI had been formed during the pre-cycling activation step at 60 °C, which facilitated the stable cycling performance near room temperature. Corresponding discharge voltage profiles showed negligible polarizations during cycling (Fig. S14b). Fig. 4f compares the onset discharging voltage of various reported polyether SPE based ASSLBs over a wide temperature range, with a typical filtering requisite of 80% theoretical capacity (Fig. S15). Among the representative polyether based SPEs, our PBO SPE demonstrates an outstanding intrinsic compatibility with high-voltage cathodes and enables a high utilization of the theoretical capacity. For further ASSLBs development, the use of rationally engineered electrodes such as vertically aligned thin electrodes [6,42], patterned lithium anodes [42,43], and other advanced composite electrodes [44–46] in combination with the PBO SPE shall possibly boost the areal capacity loading of the battery cell for practical operation near room temperature. A much thinner (~ 22 μm) PBO SPE membrane can also be obtained by using a polypropylene support instead of glass fiber (Fig. S16).

3. Conclusions

A solid polymer electrolyte based on poly(butylene oxide) was prepared by a scalable solvent-free method. Feasible room-temperature battery performance was achieved without any additional plasticizers, solvents, or liquid electrolytes. Stable cycling performance was demonstrated with a $LiFePO_4$ cathode at room temperature (~ 28 °C), delivering a stable specific capacity of ~ 140 mA h g^{-1} at 0.1 C for 100 cycles with almost 100% retention. The electrochemical activation at an elevated temperature was found to play an important role in the room-

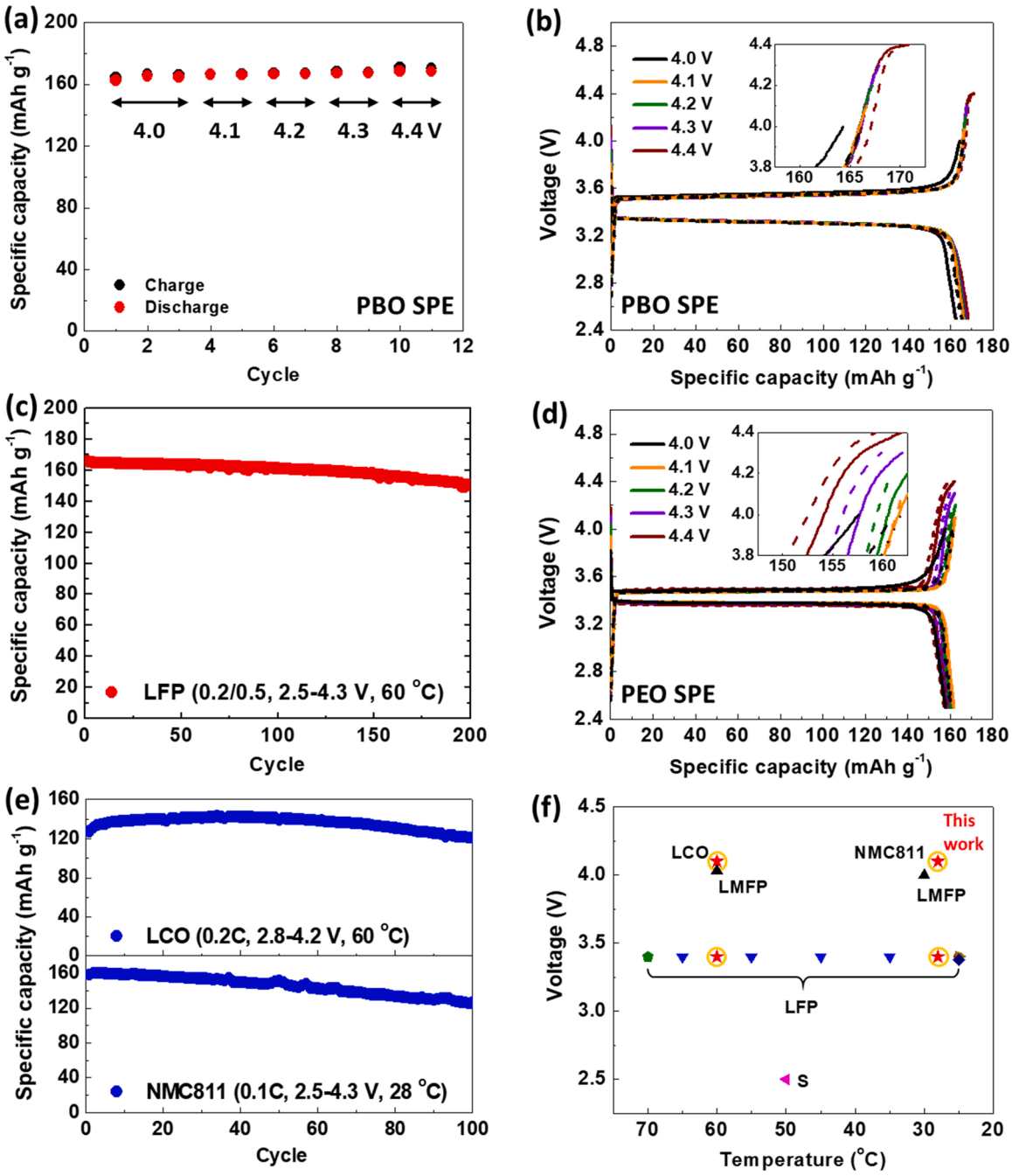

Fig. 4. Intrinsic stability of the PBO SPE toward high voltage. (a) Cycling stability of LFP/PBO SPE/Li cell upon increasing upper voltage limits from 4.0 to 4.4 V at a current density of 0.2 C at 60 °C; (b) corresponding charge-discharge profiles (inset is a magnified view for high voltages; solid line for the 1st cycle and dashed line for the 2nd cycle at each voltage limit setting). (c) Cycling performance of the LFP/PBO SPE/Li cell with an upper voltage limit of 4.3 V under a slow-charge/fast-discharge cycling protocol of 0.2 C charge and 0.5 C discharge at 60 °C. (d) Cycling charge-discharge profiles of LFP/PEO SPE/Li cell upon increasing upper voltage limits at 0.2 C and 60 °C (inset is a magnified view for high voltages; solid line for the 1st cycle and dashed line for the 2nd cycle at each voltage limit setting). (e) Cycling performance using 4-V class cathodes. (f) Comparison with representative polyether SPE based ASSLBs by initial discharge voltage [12,47–53].

temperature performance. XPS analysis confirmed the in-situ formation of a favorable CEI with rich LiF and Li_2O on the cathode surface. In addition, the PBO based SPE also exhibited better intrinsic stability toward 4-V class cathodes compared to typical PEO based SPE. Stable cycling performance was demonstrated with $LiCoO_2$ and NMC811 cathodes. Overall, the CEI enabled room-temperature performance shall revive the interests for PBO based all-solid-state batteries and provide more opportunities for dry polymer electrolytes. The PBO SPE film can reach a practical thinness by using a polypropylene separator support or other advanced SSE skeletons.

Supporting Information

Detailed experimental methods, thermogravimetric analysis, transference number determination, and additional electrochemical performance and charge-discharge curves.

CRediT authorship contribution statement

Jing Luo: Conceptualization, Methodology, Writing – original draft, Writing – review & editing, Investigation. **Qian Sun:** Conceptualization,

Methodology, Writing – review & editing. **Jianneng Liang, Xiaofei Yang, and Jianwen Liang:** Validation, Writing – review & editing. **Xiaoting Lin, Feipeng Zhao, and Yulong Liu:** Formal analysis, Writing – review & editing. **Xueling Sun:** Supervision, Writing – review & editing. All authors participated in the reviewing and editing of the manuscript.

Declaration of Competing Interest

The authors declare that they have no known competing financial interests or personal relationships that could have appeared to influence the work reported in this paper.

Acknowledgement

This research was supported by Natural Sciences and Engineering Research Council of Canada (NSERC), GLABAT Solid-State Battery Inc., China Automotive Battery Research Institute Co. Ltd, Canada Research Chair Program (CRC), Canada Foundation for Innovation (CFI), Ontario Research Fund, Canada MITACS, and University of Western Ontario.

Appendix A. Supplementary material

Supplementary data associated with this article can be found in the online version at doi:10.1016/j.nanoen.2021.106566.

References

[1] R.J. Chen, W.J. Qu, X. Guo, L. Li, F. Wu, The pursuit of solid-state electrolytes for lithium batteries: from comprehensive insight to emerging horizons, Mater. Horiz. 3 (6) (2016) 487–516.
[2] H. Zhang, J. Zhang, J. Ma, G. Xu, T. Dong, G. Cui, Polymer electrolytes for high energy density ternary cathode material-based lithium batteries, Electrochem. Energy Rev. 2 (1) (2019) 128–148.
[3] S.-J. Tan, X.-X. Zeng, Q. Ma, X.-W. Wu, Y.-G. Guo, Recent advancements in polymer-based composite electrolytes for rechargeable lithium batteries, Electrochem. Energy Rev. 1 (2) (2018) 113–138.
[4] Z. Xue, D. He, X. Xie, Poly(ethylene oxide)-based electrolytes for lithium-ion batteries, J. Mater. Chem. A 3 (38) (2015) 19218–19253.
[5] Y. Ding, Z.P. Cano, A. Yu, J. Lu, Z. Chen, Automotive Li-ion batteries: current status and future perspectives, Electrochem. Energy Rev. 2 (1) (2019) 1–28.
[6] X. Yang, Q. Sun, C. Zhao, X. Gao, K.R. Adair, Y. Liu, J. Luo, X. Lin, J. Liang, H. Huang, L. Zhang, R. Yang, S. Lu, R. Li, X. Sun, High-areal-capacity all-solid-state lithium batteries enabled by rational design of fast ion transport channels in vertically-aligned composite polymer electrodes, Nano Energy 61 (2019) 567–575.
[7] P. Hovington, M. Lagace, A. Guerfi, P. Bouchard, A.; Manger, C.M.; Julien, M.; Armand, K. Zaghib, New lithium metal polymer solid state battery for an ultrahigh energy: nano C-LiFePO4 versus nano Li1.2V3O8, Nano Lett. 15 (4) (2015) 2671–2678.
[8] J. Zheng, H. Dang, X. Feng, P.-H. Chien, Y.-Y. Hu, Li-ion transport in a representative ceramic–polymer–plasticizer composite electrolyte: Li7La3Zr2O12–polyethylene oxide–tetraethylene glycol dimethyl ether, J. Mater. Chem. A 5 (35) (2017) 18457–18463.
[9] L. Porcarelli, A.S. Shaplov, F. Bella, J.R. Nair, D. Mecerreyes, C. Gerbaldi, Single-ion conducting polymer electrolytes for lithium metal polymer batteries that operate at ambient temperature, ACS Energy Lett. 1 (4) (2016) 678–682.
[10] Y. Zhang, W. Cai, R. Rohan, M. Pan, Y. Liu, X. Liu, C. Li, Y. Sun, H. Cheng, Toward ambient temperature operation with all-solid-state lithium metal batteries with a sp3 boron-based solid single ion conducting polymer electrolyte, J. Power Sources 306 (2016) 152–161.
[11] Y. Li, F. Ding, Z. Xu, L. Sang, L. Ren, W. Ni, X. Liu, Ambient temperature solid-state Li-battery based on high-salt-concentrated solid polymeric electrolyte, J. Power Sources 397 (2018) 95–101.
[12] X.W. Li, Z.X. Zhang, S.J. Li, K.H. Yang, L. Yang, Polymeric ionic liquid-ionic plastic crystal all-solid-state electrolytes for wide operating temperature range lithium metal batteries, J. Mater. Chem. A 5 (40) (2017) 21362–21369.
[13] T. Dong, J. Zhang, G. Xu, J. Chai, H. Du, L. Wang, H. Wen, X. Zang, A. Du, Q. Jia, X. Zhou, G. Cui, A multifunctional polymer electrolyte enables ultra-long cycle-life in a high-voltage lithium metal battery, Energy Environ. Sci. 11 (2018) 1197–1203.
[14] C. Zhao, J. Liang, Q. Sun, J. Luo, Y. Liu, X. Lin, Y. Zhao, H. Yadegari, M.N. Banis, R. Li, H. Huang, L. Zhang, R. Yang, S. Lu, X. Sun, Synergistic coupling of ether electrolyte and 3D electrode enables titanates with extraordinary coulombic efficiency and rate performance for sodium-ion capacitors, Small Methods 3 (2) (2019), 1800371.
[15] P. Yao, B. Zhu, H. Zhai, X. Liao, Y. Zhu, W. Xu, Q. Cheng, C. Jayyosi, Z. Li, J. Zhu, K.M. Myers, X. Chen, Y. Yang, PVDF/palygorskite nanowire composite electrolyte for 4 V rechargeable lithium batteries with high energy density, Nano Lett. 18 (10) (2018) 6113–6120.
[16] J. Zheng, Y.-Y. Hu, New insights into the compositional dependence of Li-ion transport in polymer–ceramic composite electrolytes, ACS Appl. Mater. Interfaces 10 (4) (2018) 4113–4120.
[17] R. Hiorns, R.J. Boucher, R. Duhlev, K.H. Hellwich, P. Hodge, A.D. Jenkins, R.G. Jones, J. Kahovec, G. Moad, C. Ober, D.W. Smith, R.F.T. Stepto, J.-P. Vairon, J. Vohlidal, A Brief Guide to Polymer Nomenclature, Vol. 98, 2013, pp. 1–2.
[18] C. Sommer, J.S. Pedersen, P.C. Stein, Apparent specific volume measurements of poly(ethylene oxide), poly(butylene oxide), poly(propylene oxide), and octadecyl chains in the micellar state as a function of temperature, J. Phys. Chem. B 108 (20) (2004) 6242–6249.
[19] D.G. Mackanic, W. Michaels, M. Lee, D. Feng, J. Lopez, J. Qin, Y. Cui, Z. Bao, Crosslinked poly(tetrahydrofuran) as a loosely coordinating polymer electrolyte, Adv. Energy Mater. 8 (25) (2018), 1800703.
[20] A. Du, H. Zhang, Z. Zhang, J. Zhao, Z. Cui, Y. Zhao, S. Dong, L. Wang, X. Zhou, G. Cui, A crosslinked polytetrahydrofuran-borate-based polymer electrolyte enabling wide-working-temperature-range rechargeable magnesium batteries, Adv. Mater. 31 (11) (2019), 1805930.
[21] S. Huang, Z. Cui, L. Qiao, G. Xu, J. Zhang, K. Tang, X. Liu, Q. Wang, X. Zhou, B. Zhang, G. Cui, An in-situ polymerized solid polymer electrolyte enables excellent interfacial compatibility in lithium batteries, Electrochim. Acta 299 (2019) 820–827.
[22] Y.P. Liao, J. Liu, V. Peter, Replies to comments contained in "Conductivity hysteresis in polymer electrolytes incorporating poly(tetrahydrofuran)" by O. Akbulut et al., Electrochim. Acta 52 (2007) 1983, Electrochim. Acta 52 (24) (2007) 7173–7180.
[23] O. Akbulut, I. Taniguchi, S. Kumar, Y. Shao-Horn, A.M. Mayes, Conductivity hysteresis in polymer electrolytes incorporating poly(tetrahydrofuran), Electrochim. Acta 52 (5) (2007) 1983–1989.
[24] C.A. Furtado, G.G. Silva, M.A. Pimenta, J.C. Machado, Conductivities, thermal properties and Raman studies of poly(tetramethylene glycol) based polymer electrolytes, Electrochim. Acta 43 (10–11) (1998) 1477–1480.
[25] M. Alamgir, R.D. Moulton, K.M. Abraham, Li^{+}-conductive polymer electrolytes derived from poly(1,3-dioxolane) and polytetrahydrofuran, Electrochim. Acta 36 (5–6) (1991) 773–782.
[26] S. Das, A. Ghosh, Structure, ion transport, and relaxation dynamics of polyethylene oxide/poly (vinylidene fluoride co-hexafluoropropylene) – lithium bis (trifluoromethane sulfonyl) imide blend polymer electrolyte embedded with ionic liquid, J. Appl. Phys. 119 (2016), 095101, 95101-4785.
[27] L. Edman, Ion association and ion solvation effects at the crystalline–Amorphous phase transition in PEO–LiTFSI, J. Phys. Chem. B 104 (31) (2000) 7254–7258.
[28] B. Sun, J. Mindemark, E.V. Morozov, L.T. Costa, M. Bergman, P. Johansson, Y. Fang, I. Furo, D. Brandell, Ion transport in polycarbonate based solid polymer electrolytes: experimental and computational investigations, Phys. Chem. Chem. Phys. 18 (14) (2016) 9504–9513.
[29] L. Fan, S.Y. Wei, S.Y. Li, Q. Li, Y.Y. Lu, Recent progress of the solid-state electrolytes for high-energy metal-based batteries, Adv. Energy Mater. 8 (11) (2018).
[30] C. Fodor, A. Domján, B. Iván, Unprecedented scissor effect of macromolecular cross-linkers on the glass transition temperature of poly(N-vinylimidazole), crystallinity suppression of poly(tetrahydrofuran) and molecular mobility by solid state NMR in poly(N-vinylimidazole)-ʟ-poly(tetrahydrofuran) conetworks, Polym. Chem. 4 (13) (2013) 3714–3724.
[31] S. Motokucho, M. Furukawa, M. Kawashima, K. Kojio, K. Yoshinaga, Physical properties of poly(tetrahydrofuran)-block-poly(2-ethyl-2-oxazoline) triblock copolymer, Polym. J. 45 (11) (2013) 1115–1119.
[32] C. Fodor, G. Kali, R. Thomann, Y. Thomann, B. Iván, R. Mülhaupt, Nanophasic morphologies as a function of the composition and molecular weight of the macromolecular cross-linker in poly(N-vinylimidazole)-ʟ-poly(tetrahydrofuran) amphiphilic conetworks: bicontinuous domain structure in broad composition ranges, RSC Adv. 7 (12) (2017) 6827–6834.
[33] D.H.C. Wong, J.L. Thelen, Y. Fu, D. Devaux, A.A. Pandya, V.S. Battaglia, N. P. Balsara, J.M. DeSimone, Nonflammable perfluoropolyether-based electrolytes for lithium batteries, Proc. Natl. Acad. Sci. USA 111 (9) (2014) 3327–3331.
[34] L. Chen, Y. Li, S.-P. Li, L.-Z. Fan, C.-W. Nan, J.B. Goodenough, PEO/garnet composite electrolytes for solid-state lithium batteries: from "ceramic-in-polymer" to "polymer-in-ceramic", Nano Energy 46 (2018) 176–184.
[35] B. Sun, C. Xu, J. Mindemark, T. Gustafsson, K. Edström, D. Brandell, At the polymer electrolyte interfaces: the role of the polymer host in interphase layer formation in Li-batteries, J. Mater. Chem. A 3 (26) (2015) 13994–14000.
[36] C. Xu, B. Sun, T. Gustafsson, K. Edström, D. Brandell, M. Hahlin, Interface layer formation in solid polymer electrolyte lithium batteries: an XPS study, J. Mater. Chem. A 2 (20) (2014) 7256–7264.
[37] J.P. Contour, A. Salesse, M. Froment, M. Garreau, J. Thevenin, D. Warin, Analysis by electron-microscopy and xps of lithium surfaces polarized in anhydrous organic electrolytes, J. Microsc. Spectrosc. Electron. 4 (4) (1979) 483–491.
[38] Y. Zhu, X. He, Y. Mo, Origin of outstanding stability in the lithium solid electrolyte materials: insights from thermodynamic analyses based on first-principles calculations, ACS Appl. Mater. Interfaces 7 (42) (2015) 23685–23693.
[39] X. Yang, M. Jiang, X. Gao, D. Bao, Q. Sun, N. Holmes, H. Duan, S. Mukherjee, K. Adair, C. Zhao, J. Liang, W. Li, J. Li, Y. Liu, H. Huang, L. Zhang, S. Lu, Q. Lu, R. Li, C.V. Singh, X. Sun, Determining the limiting factor of the electrochemical stability window for PEO-based solid polymer electrolytes: main chain or terminal –OH group? Energy Environ. Sci. 13 (5) (2020) 1318–1325.

[40] Y. Xia, T. Fujieda, K. Tatsumi, P.P. Prosini, T. Sakai, Thermal and electrochemical stability of cathode materials in solid polymer electrolyte, J. Power Sources 92 (1) (2001) 234–243.
[41] X. Gao, X. Yang, M. Li, Q. Sun, J. Liang, J. Luo, J. Wang, W. Li, J. Liang, Y. Liu, S. Wang, Y. Hu, Q. Xiao, R. Li, T.-K. Sham, X. Sun, Cobalt-doped SnS2 with Dual Active Centers of Synergistic Absorption-catalysis Effect for High-S loading Li-S batteries, Adv. Funct. Mater. 29 (8) (2019), 1806724.
[42] X. Gao, X. Yang, K. Adair, J. Liang, Q. Sun, Y. Zhao, R. Li, T.-K. Sham, X. Sun, Fast charging all solid-state lithium batteries enabled by rational design of dual vertically-aligned electrodes, Adv. Funct. Mater. 30 (50) (2020), 2005357.
[43] X. Yang, X. Gao, C. Zhao, Q. Sun, Y. Zhao, K. Adair, J. Luo, X. Lin, J. Liang, H. Huang, L. Zhang, S. Lu, R. Li, X. Sun, Suppressed dendrite formation realized by selective Li deposition in all-solid-state lithium batteries, Energy Storage Mater. 27 (2020) 198–204.
[44] Y. Liu, D. Lin, Y. Jin, K. Liu, X. Tao, Q. Zhang, X. Zhang, Y. Cui, Transforming from planar to three-dimensional lithium with flowable interphase for solid lithium metal batteries, Sci. Adv. 3 (10) (2017) 0713.
[45] H. Li, D. Liu, X. Zhu, D. Qu, Z. Xie, J. Li, H. Tang, D. Zheng, D. Qu, Integrated 3D electrodes based on metal-nitrogen-doped graphitic ordered mesoporous carbon and carbon paper for high-loading lithium-sulfur batteries, Nano Energy 73 (2020), 104763.
[46] T. Wang, Q. Zhang, J. Zhong, M. Chen, H. Deng, J. Cao, L. Wang, L. Peng, J. Zhu, B. Lu, 3D Holey graphene/polyacrylonitrile sulfur composite architecture for high loading lithium sulfur batteries, Adv. Energy Mater. 11 (16) (2021), 2100448.
[47] H. Huo, Y. Chen, J. Luo, X. Yang, X. Guo, X. Sun, Rational design of hierarchical "ceramic-in-polymer" and "polymer-in-ceramic" electrolytes for dendrite-free solid-state batteries, Adv. Energy Mater. 9 (17) (2019), 1804004.
[48] D. Lin, P.Y. Yuen, Y. Liu, W. Liu, N. Liu, R.H. Dauskardt, Y. Cui, A silica-aerogel-reinforced composite polymer electrolyte with high ionic conductivity and high modulus, Adv. Mater. 30 (32) (2018), 1802661.
[49] Z. Wei, Z. Zhang, S. Chen, Z. Wang, X. Yao, Y. Deng, X. Xu, UV-cured polymer electrolyte for LiNi0.85Co0.05Al0.1O2//Li solid state battery working at ambient temperature, Energy Storage Mater. 22 (2019) 337–345.
[50] H. Huo, N. Zhao, J. Sun, F. Du, Y. Li, X. Guo, Composite electrolytes of polyethylene oxides/garnets interfacially wetted by ionic liquid for room-temperature solid-state lithium battery, J. Power Sources 372 (2017) 1–7.
[51] X.-X. Zeng, Y.-X. Yin, N.-W. Li, W.-C. Du, Y.-G. Guo, L.-J. Wan, Reshaping lithium plating/stripping behavior via bifunctional polymer electrolyte for room-temperature solid Li metal batteries, J. Am. Chem. Soc. 138 (49) (2016) 15825–15828.
[52] X. Tao, Y. Liu, W. Liu, G. Zhou, J. Zhao, D. Lin, C. Zu, O. Sheng, W. Zhang, H.-W. Lee, Y. Cui, Solid-state lithium–sulfur batteries operated at 37 °C with composites of nanostructured Li7La3Zr2O12/carbon foam and polymer, Nano Lett. 17 (5) (2017) 2967–2972.
[53] Y.-C. Jung, M.-S. Park, D.-H. Kim, M. Ue, A. Eftekhari, D.-W. Kim, Room-temperature performance of poly(ethylene ether carbonate)-based solid polymer electrolytes for all-solid-state lithium batteries, Sci. Rep. 7 (1) (2017) 17482.